

Kinetic analysis and parameter optimization of cone frustum-steel roll baling mechanism for round balers

Huinan Huang,^{1,2} Guangyu Hou,¹ Baohao Su,¹ Hao Yin,¹ Shaoshuai Xie,¹ Hui Tian,¹ Junliang Tian,³ Weizeng Lv,³ Dong Yao,³ Zhijun Lv,¹ Zijiang Fu¹

¹College of Mechanical and Electrical Engineering, Henan Agricultural University, Zhengzhou

²Key Laboratory of Swine Facilities Engineering, Ministry of Agriculture, Harbin

³College of Modern Agriculture, Lan Kao Vocational College of San Nong, Lankao, China

Corresponding author: Zhijun Lv, College of Mechanical and Electrical Engineering, Henan Agricultural University, Zhengzhou 450002, China. E-mail: lvzhijun@henau.edu.cn

Publisher's Disclaimer

E-publishing ahead of print is increasingly important for the rapid dissemination of science. The *Early Access* service lets users access peer-reviewed articles well before print/regular issue publication, significantly reducing the time it takes for critical findings to reach the research community.

These articles are searchable and citable by their DOI (Digital Object Identifier).

Our Journal is, therefore, e-publishing PDF files of an early version of manuscripts that undergone a regular peer review and have been accepted for publication, but have not been through the typesetting, pagination and proofreading processes, which may lead to differences between this version and the final one.

The final version of the manuscript will then appear on a regular issue of the journal.

Please cite this article as doi: 10.4081/jae.2026.2036

 ©The Author(s), 2026
Licensee [PAGEPress](#), Italy

Submitted: 11 November 2025

Accepted: 1 June 2026

Note: The publisher is not responsible for the content or functionality of any supporting information supplied by the authors. Any queries should be directed to the corresponding author for the article.

All claims expressed in this article are solely those of the authors and do not necessarily represent those of their affiliated organizations, or those of the publisher, the editors and the reviewers. Any product that may be evaluated in this article or claim that may be made by its manufacturer is not guaranteed or endorsed by the publisher.

Kinetic analysis and parameter optimization of cone frustum-steel roll baling mechanism for round balers

Huinan Huang,^{1,2} Guangyu Hou,¹ Baohao Su,¹ Hao Yin,¹ Shaoshuai Xie,¹ Hui Tian,¹ Junliang Tian,³ Weizeng Lv,³ Dong Yao,³ Zhijun Lv,¹ Zijiang Fu¹

¹College of Mechanical and Electrical Engineering, Henan Agricultural University, Zhengzhou

²Key Laboratory of Swine Facilities Engineering, Ministry of Agriculture, Harbin

³College of Modern Agriculture, Lan Kao Vocational College of San Nong, Lankao, China

Corresponding author: Zhijun Lv, College of Mechanical and Electrical Engineering, Henan Agricultural University, Zhengzhou 450002, China. E-mail: lvzhijun@henau.edu.cn

Abstract

To address the poor adaptivity and blockage of straw round balers, a cone frustum-steel roll baling mechanism was designed. Through stress analysis in the frustum-wheat straw interaction process, the conicity of the frustum was determined to be 32° to 63.4°. To expound the winding and axial migration law of wheat straw layers, EDEM 2024 was adopted to simulate the baling process of the cone frustum-steel roll baling mechanism. Taking the rotation speed of rolling-pressing steel rolls, frustum conicity, and axial clearance as test factors and formation time of rotating straw core as evaluation index, three-factor three-level horizontal regression response surface experiments were conducted. The regression equation was established to analyze influences of various factors on the index, the optimal parameter combination was determined: when the axial clearance, rotation speed of rolling-pressing steel rolls, and frustum conicity are 3.935 cm, 261.9 rpm, and 44.767 °, the predicted formation time is 5.237 s. The parameter combination was verified by tests, in which the formation time of a rotating straw core is 5.42 s, the formation time is 3.58 s shorter than that during operation of steel-roll baling mechanism. The research results provide a theoretical basis for the innovative design of round balers.

Key words: round baler; cone frustum-steel roll baling mechanism; kinetic analysis; parameter optimization.

Introduction

In recent ten years, the annual straw yield in China has stabilized at about 800 m (Liu, 2025; Zhang, 2021; Zhao, 2021), while straw is difficult to collect, store, transport, and utilize due to its scattered distribution, fluffiness, and strong seasonality. Crop straw was once burnt ad arbitrium, which not only wasted the resource but also polluted the environment. Straw baling machines have been used to compress fluffy straw into compact straw bales. Using these machines to achieve mechanized baling and harvest is a premise for promoting the more comprehensive utilization of straw (Cundiff *et al.*, 2024; Guo *et al.*, 2025; Li, 2022).

Existing straw baling machines mainly include square and round baling machines (square and round balers). The round baler developed in the mid-20th century has benefitted from significant developments due to its simple structure, low support power, and high efficiency. However, due to the lack of the systematic baling theory and support of comprehensive scientific experiments (Zhao *et al.*, 2019), existing round straw balers are often jammed when used to collect straw (Tang, 2007). This has necessitated action by Chinese researchers to develop efficient and applicable straw round balers. Foreign researchers have mainly studied the improvement of the baling mechanism and the application of round balers. For example, Josef Horstmann proposed a round baler with a pre-pressing chamber, in which the combination of a pre-pressing chamber and a rod-link baling mechanism achieves the continuous picking and baling (Horstmann, 2014). Biziorek and Delphigué (2011) invented an electrical steel-roll round baler that uses a motor to drive various steel rolls, obviating the need for chain transmission between steel rolls and showing advantages including a variable speed, reliable performance, and an optimized structure. Do Canto *et al.* (2011) evaluated the straw-collecting performance of cutting/chopping and pickup steel-roll round balers. Senthilkumar *et al.* (2016) assessed the performance of rice straw round balers. Chinese researchers mainly improved the baling mechanism of round balers. Wang *et al.* designed a round baler with a variable bale chamber and conducted finite element and kinematic simulation analysis to verify that material jam and accumulation do not occur during operation of the baler **Errore. L'origine riferimento non è stata trovata.** Du *et al.* (2010) theoretically analyzed the rear chamber and optimized the baling mechanism of quasi-helically arranged steel rolls. Wang *et al.* (2010) improved the round baler and added a roll-type feeding device at the feed inlet. Tests show that the addition of that roll-type feeding device can significantly improve the feeding performance of round balers. Li *et al.* (2016) studied the baling mechanism of a roll-disk round baler, and replaced the sidewall panel at the axial end with a rotary disk, which improves the baling performance and reduces energy consumption. Researchers worldwide have exerted much effort to improve

the round baler and its baling mechanism, while such innovative baling mechanisms are rarely applied in practice.

To address the aforementioned problem, the authors designed a cone frustum-steel roll baling mechanism for the steel-roll round baler. By installing a frustum-shaped core tube in one axial side of the bale chamber, the rolling-pressing pressure can be applied continuously to the straw just entering the bale chamber in the space formed by the circumferential steel rolls and the axial frustum in the baling process. Then, a large tractive force driving the winding of straw is formed on the outer surface of the straw core. The resulting torque ensures the straw to roll rapidly, wind, and ascend to form a rotating straw core, thus avoiding blockage. Through stress analysis, discrete element method simulation, and bench testing, the optimal combination of key structural and operating parameters of the baling mechanism was determined and verified by conducting comparative tests. The research provides theoretical support for the structural innovation of the steel-roll round baler.

Materials and Methods

Overall structure and working principle

Overall structural composition

The cone frustum-steel roll baling mechanism comprises rolling-pressing steel rolls, a frustum-shaped core tube, a front chamber, and a rear chamber. A schematic of the test apparatus is shown in Figure 1a. Twelve steel rolls are arranged circumferentially to form a cylindrical bale chamber with both sidewalls. The bale chamber with a diameter of 570 mm and a width of 820 mm can be divided into the front and rear chambers that are hinged by the end axle of the No. 9 rolling-pressing steel roll (Figure 2). The frustum-shaped core tube comprises key components including a spindle, a circular base plate, and a frustum, as displayed in Figure 1b. The frustum is fastened to the ribbed circular base plate by bolts, and then connected to the spindle installed on the sidewall external frame via a deep-groove ball bearing and a backstop ring. The frustum-shaped core tube must remain horizontal along the axis of the bale chamber.

Working principle

The working process of a round baler includes four sequential stages, namely, the formation of rotating straw core, circular rolling-pressing of straw, package of straw bales with a rope-winding and net-winding mechanism, and release of round straw bales (Sun *et al.*, 2022; Wang *et al.*, 2024; Shang *et al.*, 2021). The focus herein lies in clarifying the working principle of the

cone frustum-steel roll baling mechanism (Figure 2). When the mechanism works, a driving motor drives the module of steel guide rolls and the rolling-pressing steel rolls to undergo relative rotation at a certain speed ratio. Straw on the conveyor enters the bale chamber from the feeding inlet. With the rotation of the rolling-pressing steel rolls, some of the wheat straw layer ascends and is wound along cross-sections with different radii on the side face of the frustum. Under the joint action of the feed force of steel rolls and the tractive force exerted by the frustum-shaped core tube for straw, the straw rotates around the center of the bale chamber. At that moment, the frustum-shaped core tube begins to rotate passively, which produces a force that pushes wheat straw towards the other sidewall of the bale chamber. This enables faster accumulation of a small amount of straw, which facilitates the formation of a rotating straw core. As the rest of the straw is fed, circular rolling-pressing and then baling processes are finished, followed by the winding of straw bales with the rope-winding and net-winding mechanism and the final release of straw bales when lifting the rear chamber using a hydraulic mechanism.

Design of key components

Design of the frustum-shaped core tube

The frustum-shaped core tube is the key component required to accelerate the formation of rotating straw cores, and main factors influencing the straw winding and climbing performance include the angle θ between the frustum and the circular base plate (i.e. the frustum conicity). The range of θ can be determined by stress analysis, which lays the foundation for subsequent multi-factor parameter optimization experiment.

Frustum design

According to the actual spatial arrangement of the bale chamber, the height L of the frustum is 120 mm. Considering the requirement that the circular base plate fixed with the frustum cannot collide with rolling-pressing steel rolls in the bale chamber, the radius R of the large end of the frustum is 230 mm. The other structural dimensions of the frustum are determined by taking the straw of *Triticum aestivum* (wheat straw). A random wheat straw element (mass m) on the side face of the frustum was taken as the object under analysis and its stress analysis is shown in Figure 3. The rightward direction, vertically upward direction, and vertically inward direction of the frustum axis can be defined as the positive directions of the X, Z, and Y-axes, respectively (Xie *et al.*, 2025; Zhang *et al.*, 2025a; Zhang *et al.*, 2025b).

Based on the theorem of momentum, the following equilibrium relationship between the rate of change in momentum and the normal support force is derived:

$$N = q \cdot v_n \quad (\text{Eq. 1})$$

where:

$$q = \Delta m / \Delta t \quad (\text{Eq. 2})$$

$$v_n = v \sin \theta \quad (\text{Eq. 3})$$

$$v = \pi d n \quad (\text{Eq. 4})$$

The following constraints are obtained according to the equilibrium in the direction of the Z-axis:

$$N \sin \theta \geq mg \quad (\text{Eq. 5})$$

where:

$$m = q \Delta t \quad (\text{Eq. 6})$$

$$\Delta t = L / v \quad (\text{Eq. 7})$$

Substituting Eqs. (2), (3), and (4) into Eq. (1) yields:

$$N = q v \sin \theta \quad (\text{Eq. 8})$$

By substituting Eqs (8), (6), and (7) into Eq. (5):

$$v \sin^2 \theta \geq (L/v)g \quad (\text{Eq. 9})$$

The following constraints are deduced according to the equilibrium in the direction of the X-axis:

$$f \sin \theta = N \cos \theta \quad (\text{Eq. 10})$$

The critical condition for the gliding of wheat straw is:

$$f \leq \mu N \quad (\text{Eq. 11})$$

By combining Eqs. (10) and (11):

$$\frac{\cos \theta}{\sin \theta} \leq \mu \quad (\text{Eq. 12})$$

Based on the geometric constraints of the frustum:

$$r = R - L \cdot \cot \theta > 0 \quad (\text{Eq. 13})$$

where: N —the support force of the frustum (N); q —the feed amount of wheat straw, which is 1.2 kg/s; v_n —the component of the feeding rate of wheat straw along the direction of support

force (m/s); v —the feeding rate of wheat straw (m/s); θ —the frustum conicity ($^\circ$); Δm —changes in the mass of wheat straw (kg); Δt —the retention time of wheat straw in the frustum (s); d —the diameter of rolling-pressing steel rolls, which is 150 mm; n —rotation speed of rolling-pressing steel rolls, which is 260 rpm; m —mass of a wheat straw element (kg); g —the acceleration due to gravity, which is 9.81 m/s²; L —the height of the frustum (mm); f —the frictional force of rolling-pressing steel rolls on wheat straw (N); μ —the coefficient of static friction between wheat straw and 45# steel, which is 0.50; r —the radius of the small end of the frustum (mm); R —the radius of the large end of the frustum (mm).

By substituting the known parameters into Eqs. (9) and (12), and into Eq. (13) for geometric constraints, it is found that the frustum conicity is such that $32^\circ < \theta < 63.4^\circ$. The radius of the small end of frustum also varies with the angle.

Design of the spindle and circular base plate

The spindle is designed to have a diameter of 40 mm, with a total length of 930 mm in the left core. To achieve coordinative connections with the backstop cylinder, a slotted hole with the width of 8 mm and length of 400 mm was cut.

The bottom plate of a variable chamber is prepared by welding a circular steel plate and a metallic cylinder, as shown in Supplementary Figure 1. Six uniformly distributed slotted holes are cut circumferentially on the circular steel plate through laser cutting, which supports installation of side plates of variable chambers with different sizes. A circular hole with a diameter of 52 mm is set at the center of the circular steel plate. The metallic cylinder has an external diameter, an internal diameter, and a height of 80 mm, 62.2 mm, and 80 mm, the metallic cylinder is coaxially welded with the hole with the diameter of 52 mm on the circular steel plate, around which six trapezoidal rib plates are set to enhance the resistance of the frustum to axial load.

Structural design of rolling-pressing steel rolls and steel guide rolls

The rolling-pressing steel rolls and steel guide rolls are both prepared with cold-rolled plain carbon steel sheets. The module of steel guide rolls (composed of three steel guide rolls having an angle of 30° with the horizontal plane) and the rolling-pressing steel rolls separately promote pickup and rolling-pressing. To intensify the action of steel rolls on the straw, prismatic protrusions are set on the surface. During operation, all steel rolls need to rotate synchronously, so an appropriate clearance should be left between steel rolls, and the prismatic protrusions cannot interfere with each other. Therefore, the prismatic protrusions of different steel rolls are

axially misaligned. The rolling-pressing steel rolls with a diameter of 150 mm (including the prismatic protrusions), are prepared with steel sheets of 4 mm thick. Eight prismatic protrusions are uniformly distributed along the axial direction with the height of a single protrusion being 8 mm. The steel guide rolls have a diameter of 120 mm (including the prismatic protrusions), also with eight, 8-mm high, prismatic protrusions uniformly distributed along the axial direction. The fit clearances of the rolling-pressing steel rolls and the steel guide rolls are separately 25 and 20 mm.

Simulation tests of the baling process

Establishment of the discrete element model

The discrete element model of hollow flexible straw

The discrete element model of hollow flexible straw built previously by the research team was used (Huang et al., 2025), as illustrated in Figure 4. It is characterized by formation of a P1-type fiber by connecting P1 in series and a P2-type fiber by connecting P2 in series. Twelve P1-type and P2-type fibers are interleaved circumferentially to form a wheat straw model formed by 24 fibers. P1 and P2 foundational particles are represented by Bonding V2-B₁ and Bonding V2-B₂, which separately approximately simulate the bonding strength between fibers along the circumferential direction and that of the fibers themselves (Ma et al., 2023; Xie et al., 2024; Zhang et al., 2018).

Establishment of the model for the cone frustum-steel roll baling mechanism

To ensure correctness and efficiency of virtual simulations, the 3D model of the testing apparatus of cone frustum-steel roll baling mechanism designed using software SolidWorks 2024 was saved as an .stl file, imported into EDEM 2024 software and simplified (Liu et al., 2024; Mei et al., 2025; Zhao et al., 2018), as shown in Supplementary Figure 2.

Setting of simulation parameters

To explore the trends in migration of wheat straw during the formation of rotating straw cores in the bale chamber of the cone frustum-steel roll baling mechanism, the structural and motion parameters were selected for the simulation process. These included a frustum conicity of 40°, a clearance of 30 mm between the circular base plate of the frustum-shaped core tube and the sidewall (shortened as axial clearance), rotation speed of steel guide rolls of 300 rpm, rotation speed of rolling-pressing steel rolls of 270 rpm, and a conveyor speed of 1.2 m/s. Meanwhile, the feeding amount of particle factory in the pre-processing stage of simulation was set to

0.8 kg/s, and the total mass of wheat straw fed was 24 kg. In the first 1.5 s, the frustum-shaped core tube is stationary to simulate the friction between the initial small amount of wheat straw with the side face of the frustum; between 1.5 and 3.5 s, the frustum undergoes motion around the axis of the spindle at a uniform angular acceleration of 210 deg/s^2 with an initial acceleration of 0, to simulate the process in which the friction between wheat straw and the side face of the frustum gradually increases; after 3.5 s, the frustum undergoes uniform motion at an angular velocity of 420 deg/s , during which a rotating straw core is formed and rotated (Li *et al.*, 2025; Yang *et al.*, 2025). Setting of other simulation parameters is as listed in Table 1.

Results

Result analysis of simulations

To improve the simulation efficiency and verify the correctness of preliminary theoretical analysis, a work station (I9-14900K, RTX 4090 24G×1) was used to conduct comparative tests on virtual baling of the cone frustum-steel roll and steel-roll baling mechanisms. After simulation tests, a simulation post-processing module shows that in the period from 0 to 12 s, the rotating straw core has been rotated continuously. Therefore, relevant parameters in the first 12 s were ascertained and analyzed.

Analysis of flow trajectories of wheat straw

To investigate the flow and migration laws of wheat straw in the bale chamber, a wheat straw element was selected at the same position on the sidewall of the steel-roll and cone frustum-steel roll baling mechanisms. The post-processing module was adopted to export data pertaining to the spatial coordinates of the wheat straw within 5 s. Origin 2025b software was used to plot flow trajectories of the wheat straw in the two baling mechanisms, as illustrated in Figure 5. After winding and climbing the frustum for a cycle, the wheat straw marked in red shows axial migration with spiral winding towards the other sidewall; while the wheat straw marked in blue shows pure in-situ winding motion. Furthermore, the winding and formation path of the red wheat straw more resembles a circle along the diametral direction of the bale chamber than the blue one. This indicates that the introduction of the frustum-shaped core tube can not only drive wheat straw to wind and climb but also induces axial motion, allowing faster accumulation of wheat straw and contact with more rolling-pressing steel rolls. This is conducive to accelerating the formation of rotating straw cores.

Analysis of the wheat straw velocity

The post-processing function of EDEM was adopted to analyze the velocity of wheat straw fed, which is in five ranges: 0 to 0.4, 0.4 to 0.8, 0.8 to 1.2, 1.2 to 1.6, and 1.6 to 2.0 m/s. The corresponding colors are shown in Supplementary Figure 3.

Eight times (1.8, 2.0, 2.2, 2.5, 3.0, 3.5, 4.0, and 5.0 s) were selected for comparison (Figure 6). As shown in Figure 6, the wheat straw moves at an initial velocity of 0.7 m/s in the simulation and is pushed into the bale chamber by the conveyor at 1.2 m/s. The velocity of wheat straw stabilizes between 0.8 and 1.2 m/s before coming into contact with rolling-pressing steel roll G1. Both the cone frustum-steel roll and steel-roll baling mechanisms can preliminarily form a rotating straw core within the first 3.0 s. The period from 1.8 to 2.0 s is the initial throwing stage, as shown in Figure 6 a-d. The wheat straw velocity at the center of the two baling mechanisms decelerates significantly and blockages are likely to occur if wheat straw is not fed continuously. From 2.2 s to 3.0 s (Figure 6 e-j), wheat straw in the cone frustum-steel roll baling mechanism comes into contact with rolling-pressing steel rolls G1 to G7 (along with slight friction with G12 after 2.5 s and contact with G11 at 3.0 s), while that in the steel-roll baling mechanism only makes contact with rolling-pressing steel rolls G1 to G6 (along with slight friction with G7 and G12 at 3.0 s). This indicates that the cone frustum-steel roll baling mechanism is better than the steel-roll system in expanding the contact area with rolling-pressing steel rolls. Between 3.5 and 5.0 s (Figure 6 k-q), the cone frustum-steel roll baling mechanism has a smaller low-velocity area (dark and light blue) and a larger high-velocity area (red and orange) of wheat straw, than the steel-roll baling mechanism. A straw core is formed in layers at 5.0 s, and the cone frustum-steel roll baling mechanism shows better layering integrity than the steel-roll one, which exhibits obscure layering and significant of its axis.

Stress analysis of rolling-pressing steel rolls

To explore the circular winding of wheat straw driven by rolling-pressing steel rolls, changes in the total force on each rolling-pressing steel roll with time were plotted using Origin 2025b software based on data from the first 12 s extracted using the post-processing module of EDEM (Lv and Xiong, 2018), as shown in Figure 7. The force acting on rolling-pressing steel roll G1 is greater than those on other rolling-pressing steel rolls. This is mainly because G1 is in the locus of intersection of the inclined plane formed by steel guide rolls C1, C2, and C3 with the tangent of rolling-pressing steel rolls to the circumference of the bale chamber, and it needs preliminary to roll the fed wheat straw.

Figure 7 a,b shows that the stress on rolling-pressing steel rolls follows a consistent trend in both baling mechanisms, albeit with a significant discrepancy in the order of magnitude. By referring to the stress condition of rolling-pressing steel rolls G2~G12 in the period from 11 to 12 s: the stress on rolling-pressing steel rolls in the cone frustum-steel roll baling mechanism is mainly between 3000 and 5000 N, while that in the steel-roll baling mechanism is mainly between 2000 and 4000 N.

To observe the difference in the stress condition of various rolling-pressing steel rolls, 120 data points collected in the range of 0 to 12 s were integrated. Stresses on steel rolls at all data points in four intervals (0 to 6, 6 to 9, 9 to 12, and 0 to 12 s) were summed. Origin 2025b software was then adopted to plot the stresses on various rolling-pressing steel rolls in different stages, as illustrated in Figure 8.

It can be seen from Figure 8 that the red and green curves separately represent distributions of total forces on rolling-pressing steel rolls in the simulations of cone frustum-steel roll and steel-roll baling mechanisms. The force on rolling-pressing steel roll G1 is significantly higher than that on other rolling-pressing steel rolls in all stages. In the zones of rolling-pressing steel rolls G2 to G10, the forces on rolling-pressing steel rolls gradually increase in numerical order. The force decreases at first and then increases, with the minimum in the zones of rolling-pressing steel rolls G4 and G5 and large force on rolling-pressing steel roll G10. Forces on G10, G11, and G12 all decline in the first 6 s. After introducing the frustum-shaped core tube, the force on rolling-pressing steel roll G12 is lower than that on G11 while not exceeding the force on G10 between 6 and 12 s. For the steel-roll baling mechanism, the force on rolling-pressing steel roll G12 grows to some extent while does not exceed that on G11 between 6 to 12 s.

Comparison of plots arising from the two groups of simulations shows that introducing the frustum-shaped core tube can significantly increase the stress on rolling-pressing steel rolls. According to the principle of mutual action of forces, it means an increment of the normal pressure applied by rolling-pressing steel rolls on the wheat straw, and an effective increase in the active frictional force while keeping the coefficient of friction unchanged. That is to say, it guides wheat straw to contact more rolling-pressing steel rolls faster, promoting the rotating straw cores to form faster. The analysis lays a data foundation for the subsequent bending test and parameter optimization.

Baling test and parameter optimization

Establishment of the test bench for the cone frustum-steel roll baling mechanism of the round baler

A test bench was established on the basis of the original round baler. The test bench is shown in Figure 9a. A conveyor was used to replace the pickup, and the steel rolls and conveyor were separately powered by a driving motor and a conveyor motor, for which a frequency converter was separately equipped for the speed regulation. Wheat straw collected during the 2024 harvest season from Nanyang City, Henan Province, Central China, was used as the experimental material, with an average moisture content of 12.232% as measured using an LC-101-OB forced-air drying oven.

Test factors and evaluation index

According to the aforementioned simulation and single-factor pre-test results, baling tests were conducted by taking the axial clearance, rotation speed of rolling-pressing steel rolls, and frustum conicity as test factors and the formation time of a rotating straw core as the response. Therein, the frustum conicity, rotation speed of rolling-pressing steel rolls, and axial clearance are separately in the ranges of 35° to 55°, 240 to 280 rpm, and 3 to 13 cm, and the machined frustums are shown in Figure 9b. The time to formation of a rotating straw core is defined as the time from the entry of wheat straw in the bale chamber to the continuous rotation of a rotating straw core, excluding the time with rotation while at greatly fluctuating velocities.

Multi-factor test design and results

According to the Box-Behnken design scheme, three-factor three-level orthogonal rotation combination tests were performed (Chen *et al.*, 2025; Liao *et al.*, 2025; Zhao *et al.*, 2025). Coding of various factors and levels is displayed in Table 2.

The test results are listed in Table 3. The test design encompasses 13 groups of parameters, each with three repeated tests. Considering the interaction of various factors, a mathematical model of the test index and various factors was built and subjected to variance analysis and response surface analysis.

Analysis of test results: influences of test factors on the time to formation of a rotating straw core

Establishment of the regression model for the formation time of a rotating straw core

Based on the test results, a regression model for the formation time of a rotating straw core and various factors was established, as expressed by Eq. (14):

$$T = 6.35 + 2.72X_1 - 0.1650X_2 + 0.0688X_3 + 1.67X_1^2 + 0.8517X_2^2 + 1.43X_3^2 \quad (\text{Eq. 14})$$

By using Design Expert 12.0.3.0 software, the data were subjected to variance analysis, as shown in Table 4.

According to Eq. (14) and Table 4, X_1 , X_1^2 , and X_3^2 are all extremely significant and X_2^2 is significant. This means that the axial clearance exerts an extremely significant influence on the time to form of a rotating straw core; the secondary terms are listed (in descending order of influence on formation time) as follows: the axial clearance, frustum conicity, and rotation speed of rolling-pressing steel rolls. The coefficient of determination R^2 is 0.938, the variance of the model is approximate to 1, which suggests that the regression model is extremely significant. The lack-of-fit P is greater than 0.05 and the coefficient of variation is 9.16%, indicative of high reliability of the test (Zhang *et al.*, 2022).

Tests of the regression model for the formation time of a rotating straw core

The reliability of the regression model for the formation time of a rotating straw core was tested. The normal distribution probability graph for the residual of the regression model is illustrated in Figure 10a. Data in the figure suggest that the residual of the model is normally distributed, indicative of a high goodness of fit and excellent applicability of the regression model. Figure 10b displays the scatter plots for the actual and predicted formation times of a rotating straw core. The scatters are distributed in a quasi-linear manner, implying the high correlation between the actual and predicted values of the formation time and a small test error. Figure 10c shows the distributions of the residual and predicted value. The scatters are dispersed without obvious regularity, indicating good regression achieved by the model.

Analysis of factors influencing the formation time of a rotating straw core

The curves illustrating perturbation for the influences of various factors on the formation time of a rotating straw core are depicted in Supplementary Figure 4 (A, B, and C separately correspond to X_1 , X_2 , and X_3).

As shown in Supplementary Figure 4, the formation time of a rotating straw core decreases with decreasing axial clearance; decreases at first, then increases with the increase in the rotation speed of rolling-pressing steel rolls; and also decreases at first, then increases as the frustum conicity is increased.

Response mechanisms of the main and secondary effects of three factors to the formation time of a rotating straw core

Software Design Expert 12.0.3.0 was used to plot the response surface for the influences of main and secondary effects of three factors on the formation time of a rotating straw core, as displayed in Supplementary Figure 5. Results show that when the axial clearance is 8 cm, the response surface of the rotation speed of rolling-pressing steel rolls and the frustum conicity for the formation time of a rotating straw core is concave, with the minimum found at 260 rpm and 45°; at a rotation speed of rolling-pressing steel rolls of 260 rpm, the influences of the axial clearance and the frustum conicity on the formation time are minimum when they are separately 3 to 5 cm and 45°; when the frustum conicity is 45°, the minimum occurs when the axial clearance and the rotation speed of rolling-pressing steel rolls are separately 3 to 5 cm and 260 rpm.

Experimental verification of the optimal parameters

As revealed by the analysis of influences of various factors on the formation time of a rotating straw core and taking the formation time of a rotating straw core as the objective, the optimal parameters are obtained, including the axial clearance, rotation speed of rolling-pressing steel rolls, and frustum conicity separately being 3.935 cm, 261.938 rpm, and 44.767°, for which the formation time is predicted to be 5.237 s. Under the optimal parameter combination, the verification test for the baling of straw bales was performed under conditions same as above. The test was repeated for five groups, with 5 kg of wheat straw fed in each group. The test results are summarized in Table 5.

Test results show that rotating straw cores are all formed smoothly in the five test groups, and the straw bales rotate at a uniform angular velocity within an extremely short time. The average formation time of a rotating straw core is 5.42 s, which shows an error of 3.49% with the predicted time, thus validating the accuracy of the model prediction. Through rope winding of the formed straw bales with manual assistance, complete straw bales were obtained (Coppola *et al.*, 2025; Yin *et al.*, 2023), as shown in Supplementary Figure 6.

In the meantime, the frustum-shaped core tube was dismantled to perform five repeated baling tests on a steel-roll round baler at the same rotation speed of rolling-pressing steel rolls under the same feeding condition of wheat straw. Test results reveal that the average time taken from feeding to continuous rotation of the rotating straw core (with no significant interruption) is 9 s. The introduction of the cone frustum-steel roll baling mechanism effectively shortens the

formation time of a (continuously) rotating straw core and provides a favorable solution to the jams affecting the baling process of round balers.

Discussion

The author established a discrete element model of hollow flexible straw and applied it to the experimental study of virtual baling. In the early stage, the reliability and correctness of the model were determined by calibration research (Huang *et al.*, 2025), which ensured the authenticity of the simulation results of virtual baling. While Zhao *et al.* (2018) simulate the operation process of the feeding device of the round baler based on the solid rice straw discrete element model, the author optimized the establishment method of straw discrete element, which laid a theoretical method support for the analysis of crop straw-mechanical interaction process. In order to accelerate the formation time of rotating straw core and avoid the blockage of straw, the author puts forward the scheme of adding frustum-shaped core tube on one side of the axial direction in the traditional steel-roll round baler baling chamber. This is obviously different from the structural optimization scheme of the circumferential variable bale chamber proposed in the previous literature, which focuses on the design and kinematics simulation of the variable bale chamber device. In this paper, the design of the cone frustum-steel roll baling mechanism, the simulation of the baling process and the experiment test are carried out by means of dynamic analysis, virtual simulation and parameter optimization, which verifies the correctness of the theoretical analysis and simulation technology. In the future, the parameters of the cone frustum-steel roll baling mechanism will continue to be optimized to improve the density and density uniformity of the bales, and provide technical reference for the innovative research and development of the straw baler.

In this study, straw moisture content was treated as a controlled variable rather than an independent experimental factor. The average moisture content of the wheat straw used in the tests was 12.232%, as measured using an LC-101-OB forced-air drying oven. The focus of this study was to design a cone frustum-steel roller baling mechanism and to analyze the effects of its key structural and operational parameters on baling performance. Future studies will further investigate the multifactorial effects of different straw moisture contents and key baling-mechanism parameters on baling performance.

Conclusions

- 1) A cone frustum-steel roll baling mechanism was designed. Through stress analysis in the frustum-wheat straw interaction process in the frustum-shaped core tube, a stress model for a

wheat straw element in the baling process was established and the frustum conicity was determined to be 32° to 63.4°. The structural dimensions of other key components were ascertained with objectives to accelerate the formation of a rotating straw core and avoid jamming of the feeding inlet.

2) Software EDEM 2024 was utilized to conduct comparative simulation tests on the cone frustum-steel roll and the conventional steel-roll baling mechanisms: these reveal the winding and climbing behavior of wheat straw driven by the frustum and rolling-pressing steel rolls together in the bale chamber, verifying the conclusion that the cone frustum-steel roll baling mechanism can form a rotating straw core faster than a conventional steel-roll system. The ranges of key factors influencing the baling performance were determined through pre-test analysis.

3) Through three-factor three-level orthogonal regression tests, the optimal parameter combination of the cone frustum-steel roll baling mechanism was obtained as follows: the axial clearance is 3.935 cm, the rotation speed of rolling-pressing steel rolls is 261.938 rpm, and the frustum conicity is 44.767°, under which the predicted formation time of a rotating straw core is 5.237 s. By conducting verification tests using the optimal parameter combination, the average formation time of a rotating straw core was found to be 5.42 s, representing a discrepancy of 3.49% from the predicted value. On average, this is 3.58 s faster than the time taken to form a rotation straw core when using the conventional steel-roll baling mechanism. The research provides a theoretical basis and data support for the subsequent optimal design of round balers.

Contributions: **Huinan Huang, Zhijun Lv**, conceptualization, methodology, project administration, funding acquisition, writing – review & editing. **Guangyu Hou**, software, validation, writing – review & editing. **Guangyu Hou, Baohao Su**, formal analysis, writing – review & editing. **Huinan Huang, Guangyu Hou**, writing – original draft, writing – review & editing. **Hao Yin, Shaoshuai Xie, Hui Tian, Junliang Tian, Weizeng Lv, Dong Yao, Zijiang Fu**, writing – review & editing. All authors have read and agreed to the published version of the manuscript.

Funding: This research was funded by National Natural Science Foundation of China [grant number 52205261], the Henan Province Science and Technology Research Project [grant number 252102110350] and the Henan Province Science and Technology Research Project [grant number 252102111177].

Data Availability Statement: The data used to support the findings of this study are available from the corresponding author upon request.

Acknowledgments: The authors would like to thank their college and the laboratory, as well as gratefully appreciate the reviewers who provided helpful suggestions for this manuscript.

Conflicts of Interest: The authors declare no conflict of interest.

References

- Biziorek S, Delphigué D, 2011. Round baler with electrically driven roller. United States Patent Registration US8807023B2.
- Chen LQ, Zhu JW, Liu C, 2025. [Optimal design and test of wheat plot breeding threshing device].[Article in Chinese with English abstract]. *Trans Chin Soc for Agric Mach* 56:72-81.
- Coppola F, Ruffin A, Meneghetti G, 2025. In-field load acquisitions on a variable chamber round baler using instrumented hub carriers and a dynamometric towing pin. *Appl Sci* 15:8579.
- Cundiff SJ, Grisso DR, Webb GE, 2024. Cost comparison for emerging technologies to haul round bales for the biorefinery industry. *AgriEngineering* 6:1549-1567.
- Do Canto JL, Klepac J, Rummer R, Savoie P, Seixas F, 2011. Evaluation of two round baling systems for harvesting understory biomass. *Biomass Bioenergy* 35:2163-2170.
- Du R, Zhang H, Li D, 2010. Experiment and research on forming box of wound bundler. *J North China Inst Aerosp Eng* 20:1-3.
- Guo Q, Zhuang Y, Xu H, Li W, Li H, Wu Z, 2025. Optimization of the screw conveyor device based on a GA-BP neural network. *Machines* 13:24.
- Horstmann J, 2014. Agricultural round baler with height-adjustable shaping and pressing channel. United States Patent Registration US-8910460.
- Huang H, Zhang Y, Hou G, Su B, Yin H, Fu Z, et al., 2025. Establishment of hollow flexible model with two types of bonds and calibration of the contact parameters for wheat straw. *Agriculture* 15:1686.
- Li M, 2022. Promotion and application of wheat straw mechanical picking and baling. *Mod Agric Mach* 1:24-25.
- Li W, Zhao WJ, Zhu H, Zhai L, He X, 2025. [Design and experiment of variable pitch potato grading devices based on DEM-MBD coupling].[Article in Chinese with English abstract]. *Trans Chin Soc for Agric Mach* 56:94-104.
- Li Y, Wang D, Li D, Wang M, 2016. [Theoretical analysis and experiment of baling mechanism of roll-disk round baler].[Article in Chinese with English abstract]. *Trans Chin Soc for Agric Mach* 47:45-52.
- Liao Y, Wu A, Liao Q, Zheng J, Wang C, Zhang Q, 2025. [Design and experiment of pneumatic fertilizer discharging system for high speed seeder for rapeseed and wheat].[Article in Chinese with English abstract]. *Trans Chin Soc for Agric Mach* 56:60-71.
- Liu L, Wang X, Zhong X, Zhang X, Geng Y, Zhou H, Chen T, 2024. Design and experiment of furrow side pick-up soil blade for wheat strip-till planter using the discrete element method. *J Agric Eng* 55:1546.
- Liu X, 2025. The comprehensive utilization of crop straws. *Hebei Agric Mach* 2:91-93.
- Lv B, Xiong F, 2018. An analysis and simulation on meshing force of main chain drive in baling process of round balers. *IOP Conf Ser Earth Environ Sci* 170:042092.
- Ma Z, Zhao Z, Quan W, 2023. Calibration of discrete element parameter of rice stubble straw based on EDEM. *J Agric Sci Technol* 25:103-113.

- Mei F, Li B, Xu Z, Li X, Zhu X, 2025. Discrete element modeling of straw bale: An innovative approach to simulate the compression mechanics of fiber-based materials. *Comput Electron Agric* 231:110002.
- Senthilkumar T, Kavitha R, Shridar B, 2016. Performance evaluation of round type rice straw balers. *Indian J Agric Sci* 86:130-132.
- Shang Y, Meng Z, Cong Y, Dong J, Luo C, Song Z, 2021. Development of a control system with remote monitoring function for round baler. *Comput Electron Agric* 182:106044.
- Sun Q, Wang P, Shi S, 2022. The round baler modeling design based on unconscious quantification. *Appl Nanosci* 13:1-12.
- Tang Z, 2007. Design of large interior spiral wound bundler. *China Dairy Cattle* 4:42-45.
- Wang C, Han M, Gong Z, 2022. Structural design and simulation analysis of baler with variable bale chambers. *J Chin Agric Mech* 43:1-6.
- Wang D, Jiang Y, Wang J, 2010. [Structure-improving and experiment of steel-roll round baler].[Article in Chinese with English abstract]. *Trans Chin Soc for Agric Mach* 41:84-88.
- Wang J, Li X, Huang W, Wu L, Cui J, Bai H, Zeng F, 2024. Mathematical model for bale-density prediction in large steel roller-type round balers during bale rolling. *Bioresour Technol* 396:130445.
- Xie J, Zhang H, Feng H, Huang W, Jin J, Ma W, 2025. [Design and experiment of friction adjustable precision seed feeder device for wheat experimental sowing].[Article in Chinese with English abstract]. *Trans Chin Soc for Agric Mach* 56:164-173.
- Xie W, Ouyang C, Jiang P, Meng D, Luo H, 2024. [Calibrating and optimizing the discrete element parameters for clamping section stems during rape shoot harvesting].[Article in Chinese with English abstract]. *T CSAE* 40:104-116.
- Yang Q, Lü Z, Yan Y, Yang S, Li F, Song Z, Chen Y, 2025. [Optimization design and experiment of vertical rotary harrow for mulberry plantation].[Article in Chinese with English abstract]. *Trans Chin Soc for Agric Mach* 56:210-220.
- Yin J, Chen Z, Liu C, Zhou M, Liu L, 2023. Design and experiments of a real-time bale density monitoring system based on dynamic weighing. *Sensors (Basel)* 23:1778.
- Zhang J, Feng B, Yu X, Zhao C, Li H, Kan Z, 2022. Experimental study on the crushing properties of corn stalks in square bales. *Processes* 10:168.
- Zhang Q, 2021. [Analysis of straw burning and comprehensive utilization].[Article in Chinese with English abstract]. *Agric Henan* 19:7-8.
- Zhang Q, Qi T, Yan H, Liao Q, Du W, Cai J, 2025a. [Design and experiment of rape direct seeding straw mulching returning device in rice stubble field].[Article in Chinese with English abstract]. *Trans Chin Soc for Agric Mach* 56:186-196.
- Zhang T, Liu F, Zhao M, Ma Q, Wang W, Fan Q, Yan P, 2018. Determination of corn stalk contact parameters and calibration of discrete element method simulation. *China Agric Univ J Soc Scie Ed* 23:120-127.
- Zhang Y, Hao Z, Xu T, Diao P, Zhou H, Mei W, 2025b. [Design and experiment of dynamic compensation adaptive straw removal device for corn no-till seeder].[Article in Chinese with English abstract]. *Trans Chin Soc for Agric Mach* 56:174-185.
- Zhao P, Deng M, Wang M, Wang Z, Tuo J, Liu Z, et al., 2025. [Design and experiment of pneumatic swash plate wheat wide-seedling-belt uniform sowing device].[Article in Chinese with English abstract]. *Trans Chin Soc for Agric Mach* 56:38-47.
- Zhao R, Cao J, Zhu T, 2021. [Analysis on the international trade and competitiveness of Chinese wheat].[Article in Chinese with English abstract]. *J Chuzhou Univ* 23 14-19+41.
- Zhao X, Yang L, Dai X, Zhang N, Guo X, Dong J, et al., 2019. Research status and development trend of wheat straw round balers. *Agric Eng* 9:4-28.

Zhao Z, Huang H, Yin J, Yang SX, 2018. Dynamic analysis and reliability design of round baler feeding device for rice straw harvest. *Biosyst Eng* 174:10-19.

Supplementary Online Material.

Figure S1. Structural schematic for the circular base plate.

Figure S2. Simplified model of the cone frustum-steel roll baling mechanism.

Figure S3. Color comparison in the analysis of wheat straw velocity.

Figure S4. Perturbation curves for the influences of various factors on the formation time of a rotating straw core.

Figure S5. Response surfaces for the influences of the main and secondary effects of three factors on the formation time of a rotating straw core.

Figure S6. Experimental verification of the cone frustum-steel roll baling mechanism.

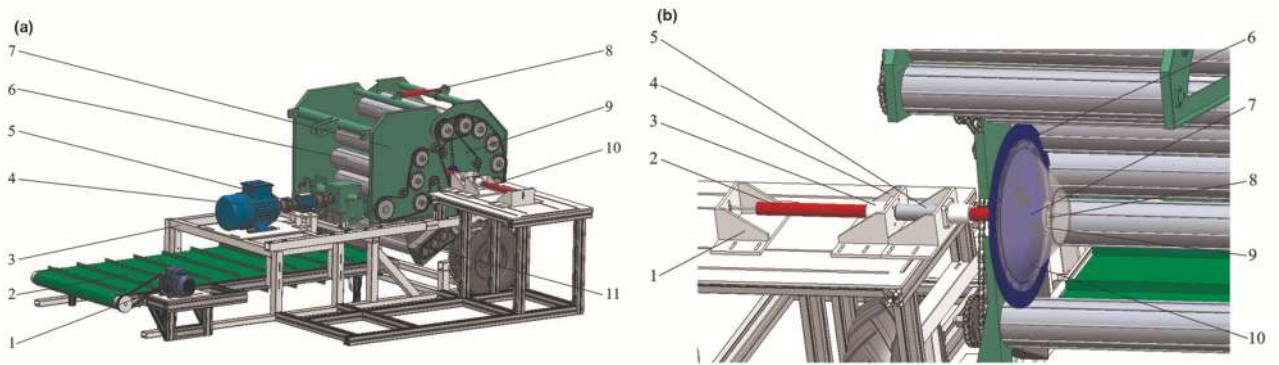


Figure 1. Schematic of the apparatus used to test the baling mechanism of the round baler. **a)** 3D model of the test apparatus; **b)** 3D model of the frustum-shaped core tube.

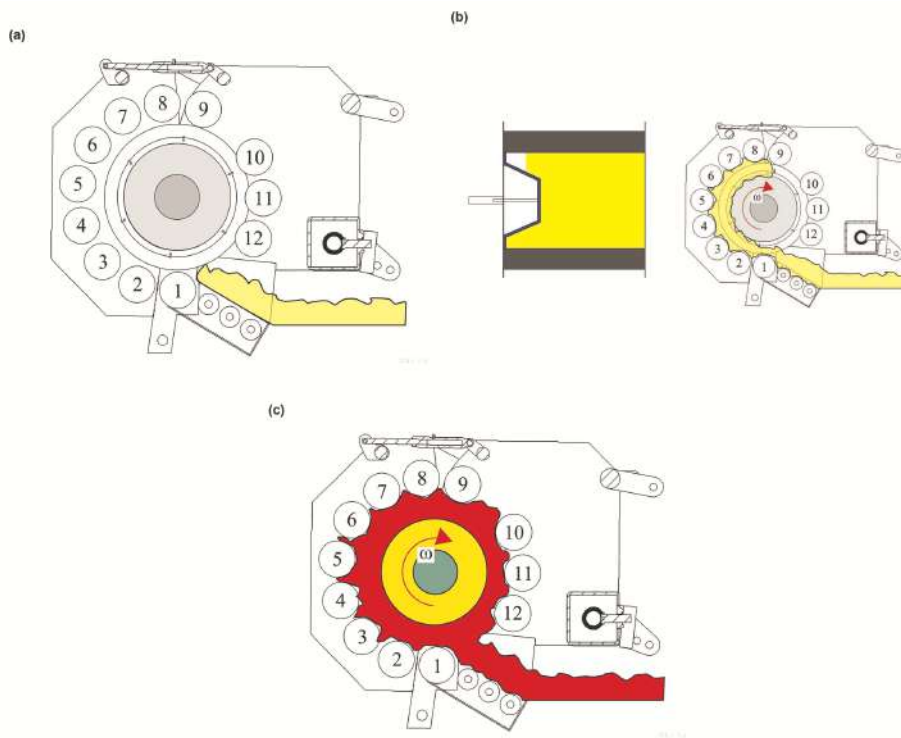


Figure 2. Schematic for the operation process of the cone frustum-steel roll baling mechanism of the steel-roll round baler. **a)** Feeding stage. **b)** Formation stage of rotating straw cores. **c)** Circular rolling-pressing stage.

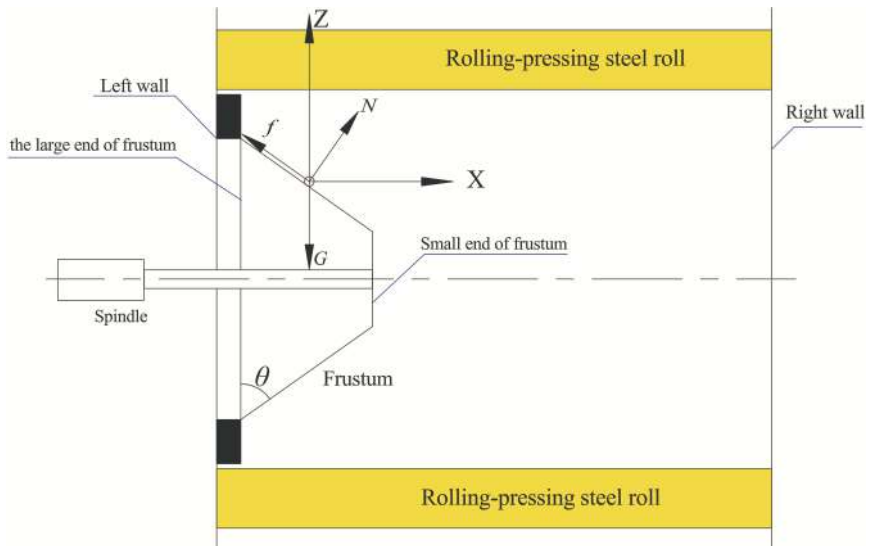


Figure 3. Stress analysis of the frustum.

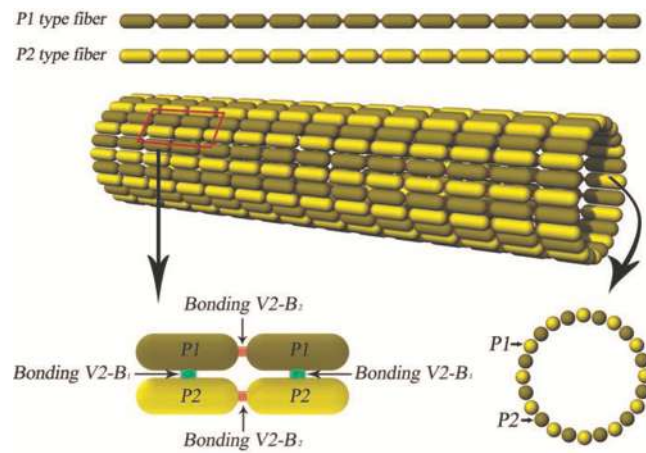


Figure 4. Discrete element model of a wheat straw.

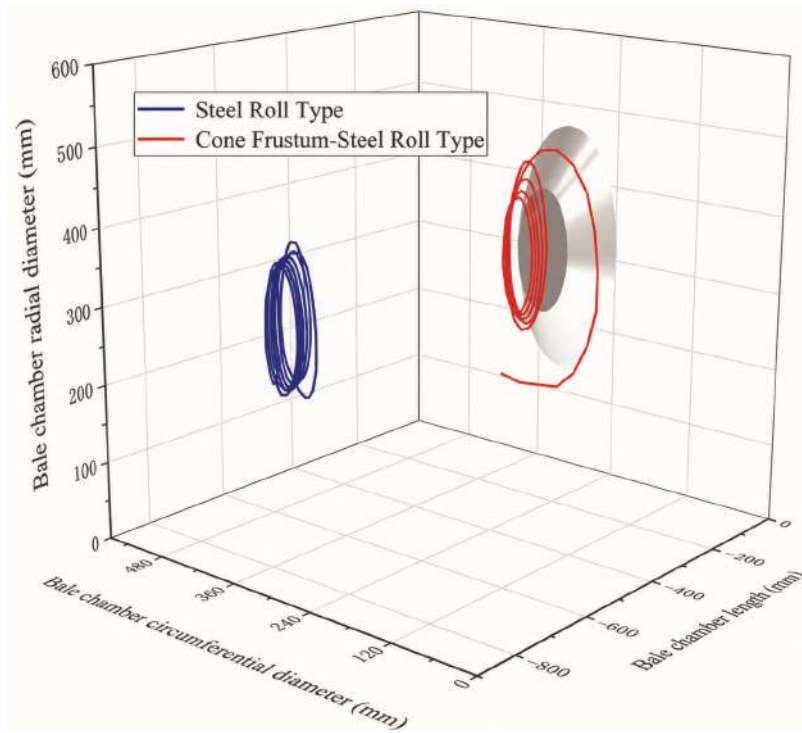


Figure 5. Flow trajectories of the wheat straw.

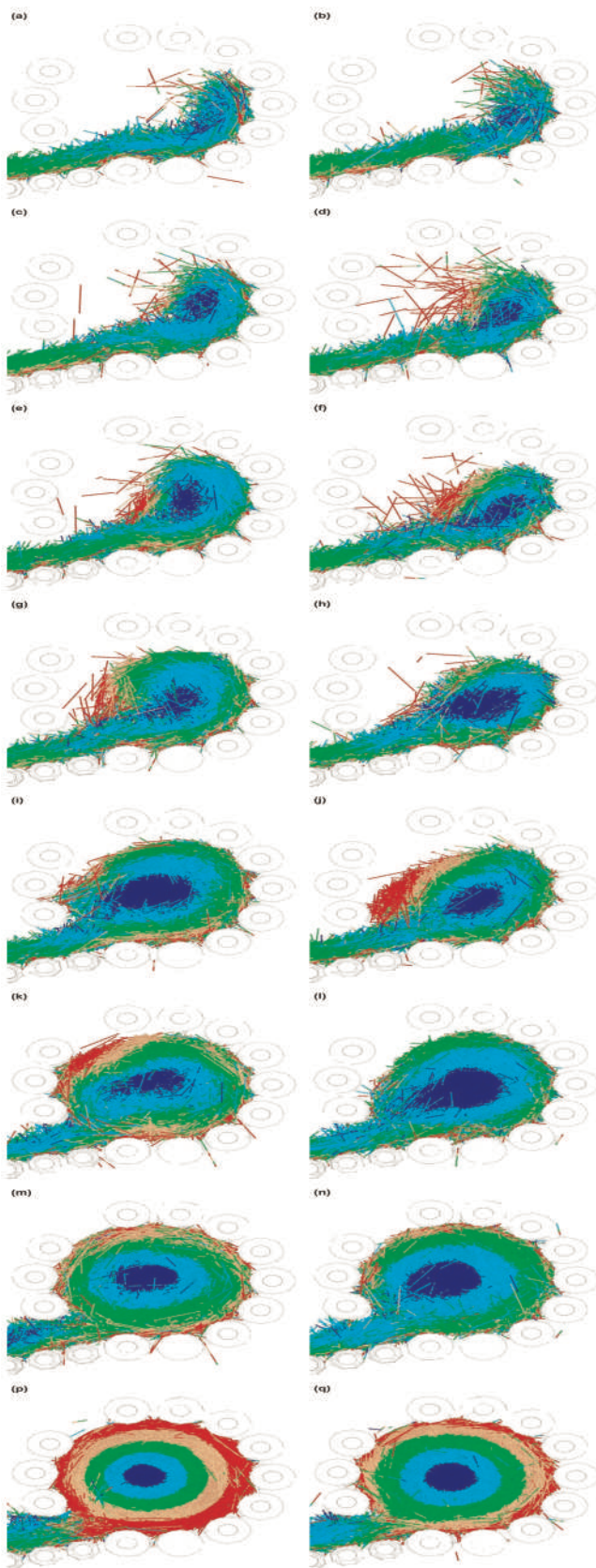


Figure 6. Analysis and comparison of wheat straw velocities. **a)** Cone frustum-steel roll baling mechanism, $t = 1.8$ s. **b)** Steel-roll baling mechanism, $t = 1.8$ s. **c)** Cone frustum-steel roll baling mechanism, $t = 2.0$ s. **d)** Steel-roll baling mechanism, $t = 2.0$ s. **e)** Cone frustum-steel roll baling mechanism, $t = 2.2$ s. **f)** Steel-roll baling mechanism, $t = 2.2$ s. **g)** Cone frustum-steel roll baling mechanism, $t = 2.5$ s. **h)** Steel-roll baling mechanism, $t = 2.5$ s. **i)** Cone frustum-steel roll baling mechanism, $t = 3.0$ s. **j)** Steel-roll baling mechanism, $t = 3.0$ s. **k)** Cone frustum-steel roll baling mechanism, $t = 3.5$ s. **l)** Steel-roll baling mechanism, $t = 3.5$ s. **m)** Cone frustum-steel roll baling mechanism, $t = 4.0$ s. **n)** Steel-roll baling mechanism, $t = 4.0$ s. **p)** Cone frustum-steel roll baling mechanism, $t = 5.0$ s. **q)** Steel-roll baling mechanism, $t = 5.0$ s.

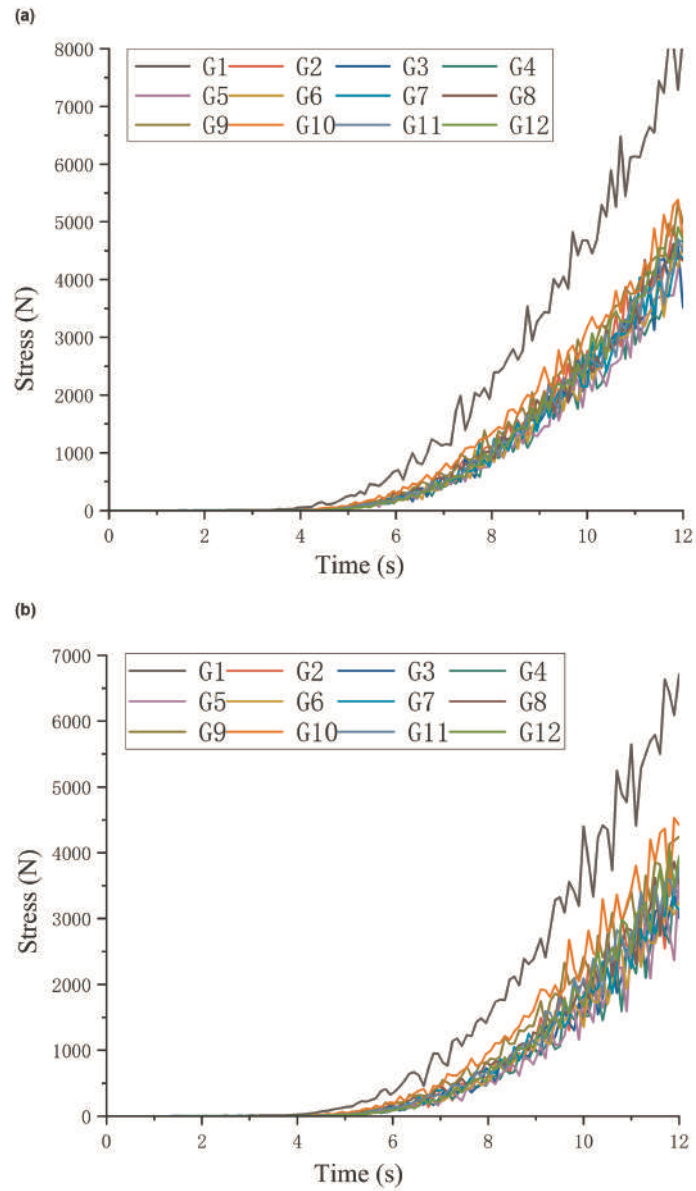


Figure 7. Stress curves of rolling-pressing steel rolls. **a)** Stress-time curves of rolling-pressing steel rolls in the cone frustum-steel roll baling mechanism. **b)** Stress-time curves of rolling-pressing steel rolls in the steel-roll baling mechanism.

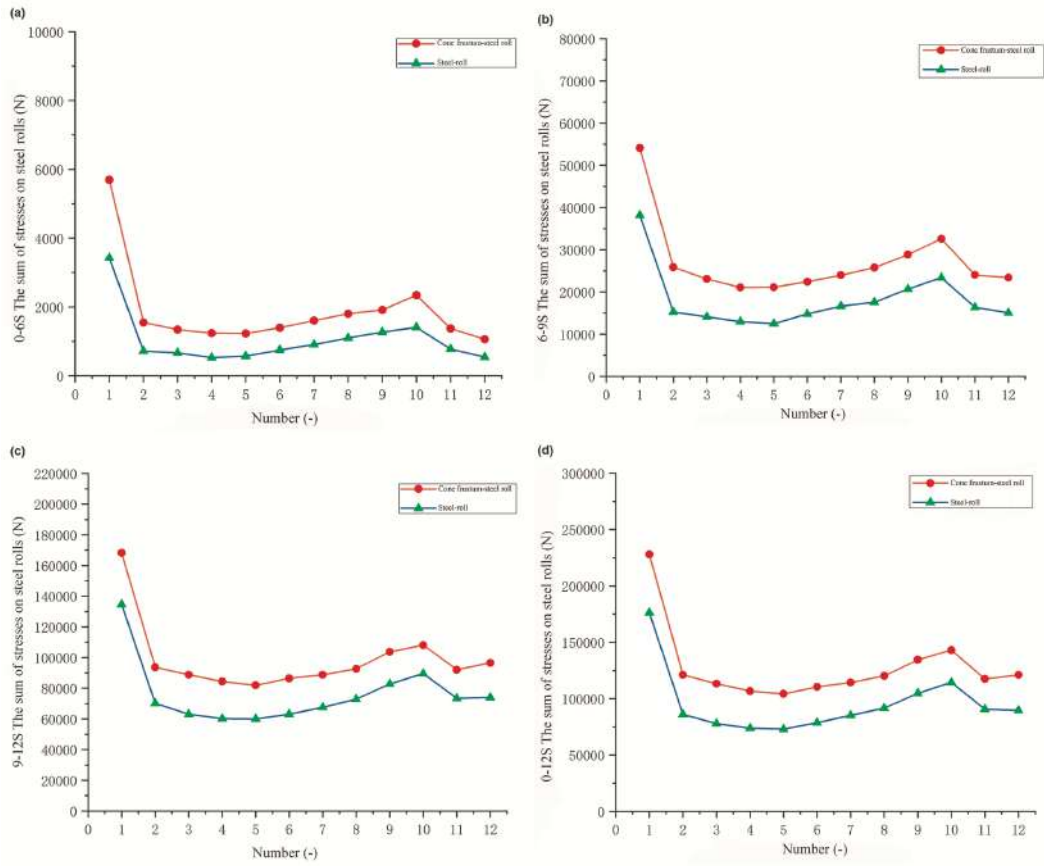


Figure 8. Sum of stresses on steel rolls in various stages. **a)** 0-6 s. **b)** 6-9 s. **c)** 9-12 s. **d)** 0-12 s.

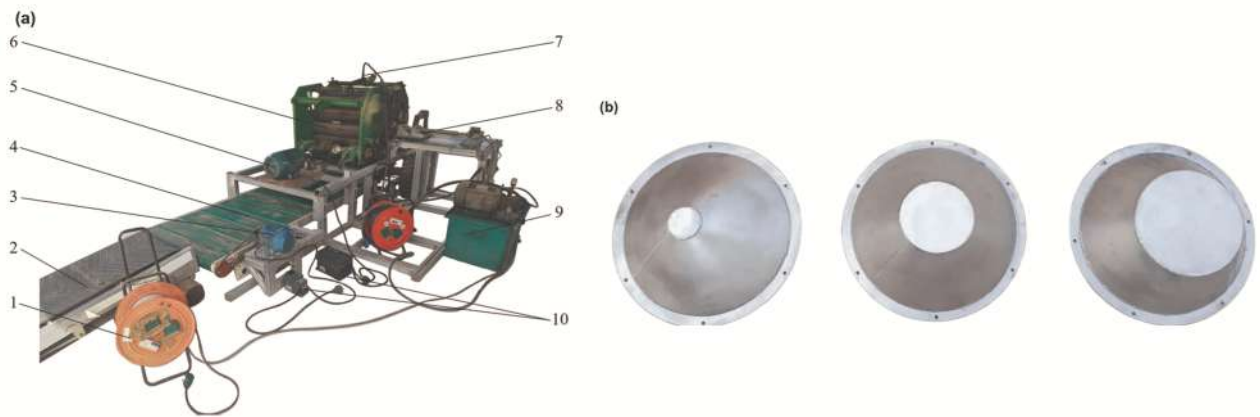


Figure 9. Physical test bench for the cone frustum-steel roll baling mechanism. **a)** Establishment of the test apparatus. **b)** Pictures of real frustum.

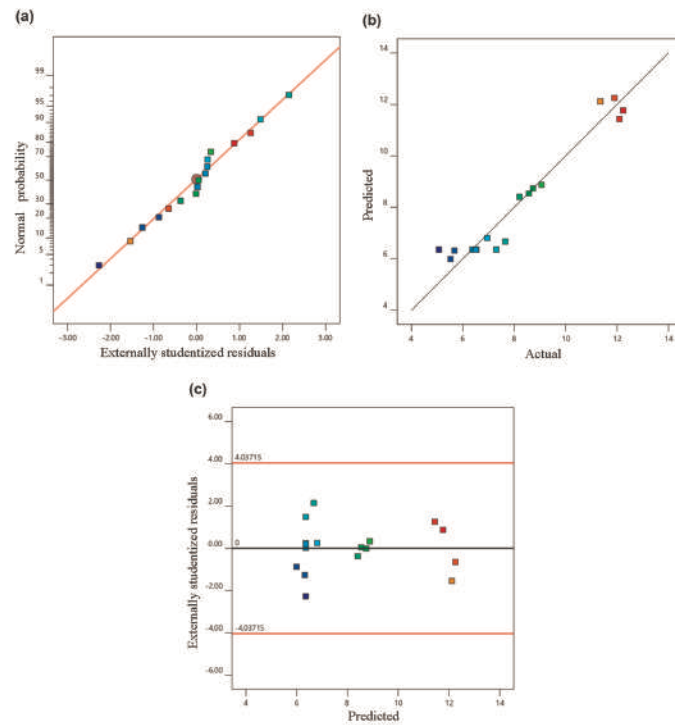


Figure 10. Test data of the regression model for the formation time of a rotating straw core. **a)** Normal distribution probability graph for the residual for the formation time of a rotating straw core. **b)** Scatter plot for the actual and predicted values of the formation time of a rotating straw core. **c)** Distributions of the residual and predicted value of formation time of a rotating straw core.

Table 1. Setting of other simulation parameters.

Type	Parameter	Value
45# steel (the frustum and steel rolls)	Density, ρ ($\text{kg}\cdot\text{m}^{-3}$)	7850
	Poisson's ratio, ν_f	0.3
	Shear modulus, G_s (Pa)	4×10^6
	Coefficient of restitution, e_s	0.479
Wheat straw-wheat straw	Coefficient of static friction, μ_s	0.227
	Coefficient of rolling friction, μ_t	0.136
	Coefficient of restitution, e_{ss}	0.482
Wheat straw-45# steel	Coefficient of static friction, μ_{ss}	0.271
	Coefficient of rolling friction, μ_{tt}	0.093

Table 2. Design of test factors for the physical test bench of the cone frustum-steel roll baling mechanism.

Level	Factors		
	X_1 /Axial clearance/cm	X_2 /Rotation speed/rpm	X_3 /Frustum conicity/ $^\circ$
-1	3	240	35
0	8	260	45
1	13	280	55

Table 3. BBD test design and results.

Test number	X_1 /cm	X_2 /rpm	X_3 / $^\circ$	T/formation time of a rotating straw core/s
1	8	240	35	8.73
2	8	260	45	6.53
3	13	260	55	11.90
4	3	240	45	5.67
5	3	260	35	7.65
6	13	260	35	11.35
7	8	280	55	8.57
8	3	280	45	5.52
9	8	260	45	6.50
10	3	260	55	6.95
11	8	260	45	5.07
12	8	240	55	9.06
13	8	260	45	6.37
14	13	280	45	12.09
15	8	280	35	8.20
16	13	240	45	12.24
17	8	260	45	7.30

Table 4. Variance analysis of the regression model for the formation time of a rotating straw core.

Source of variation	Sum of squares	Degree of freedom	Mean square	F-value	<i>p</i> -value
Model	85.64	6	14.27	25.21	< 0.0001**
X ₁	59.35	1	59.35	104.82	< 0.0001**
X ₂	0.2178	1	0.2178	0.3847	0.549
X ₃	0.0378	1	0.0378	0.0668	0.8013
X ₁ ²	11.8	1	11.8	20.84	0.001**
X ₂ ²	3.05	1	3.05	5.39	0.0426*
X ₃ ²	8.66	1	8.66	15.3	0.0029**
Residual	5.66	10	0.5662		
Lack of fit	3.07	6	0.511	0.7874	0.6228
Pure error	2.6	4	0.649		
Total	91.3	16			

R² = 93.80%; Adj R² = 90.08%; (2) ** *p*<0.01; **p*<0.05.

Table 5. Verification test results.

	1	2	3	4	5	Average
Formation time of a rotating straw core/s	5.39	5.31	5.46	5.45	5.49	5.42